A Biomimetic Multichannel Synergistic Calibration for Event-Driven Functional Electrical Stimulation

A Biomimetic Multichannel Synergistic Calibration for Event-Driven Functional Electrical Stimulation

Nicolò Landra, Andrea Prestia, Andrea Mongardi, Fabio Rossi, Danilo Demarchi, Paolo Motto Ros
Dipartimento di Elettronica e Telecomunicazioni, Politecnico di Torino, Torino, Italy, Email: nicolo.landra@polito.it

***Abstract*—In this paper, we present the Profile Extraction (PE) algorithm, which allows the computation of a multi-channel profile highly correlated with voluntary muscle activity. This event-based profile can be used as biomimetic control during the calibration phase of a Functional Electrical Stimulation (FES) system. The adoption of the PE technique represents the preliminary step to extend the applicability of our event-driven paradigm to control the coordinated multi-joint movements. Through an experimental campaign, we tested the improvements made by the use of PE in the FES calibration, assessing the reproducibility between the voluntary and stimulated movements. Results show a 2 % increase of the median correlation value for a single-channel exercise and a 3.6 % increase for a dual-channel one. A statistical decrease of normalized Root Mean Square Error has been obtained for the dual-channel exercise ($p < 0.05$).**

***Index Terms*—Event-driven Signal Processing, Functional Electrical Stimulation, Rehabilitation Engineering, Synergistic Muscular Activity**

I. Introduction

Functional Electrical Stimulation (FES) is a technique that exploits low-energy electrical pulses for generating coordinated body movements [1]. It can be used in patients affected by neuromuscular disorders as a permanent neuroprosthesis [2], [3] or as a short-term therapy to restore lost functions [4], [5]. In recent years, the applicability of FES has been extended from limited single-channel tasks to broad daily life applications (e.g., reaching and gait) [6]–[8], which involve the synergistic activation of multiple muscle groups. In this scenario, the adoption of a multi-channel FES strategy is fundamental. As several works have demonstrated [8]–[11], the FES therapeutic performance can be significantly enhanced by controlling the stimulation through biomimetic strategies, making the therapy compatible with the sensorimotor system. In this scope, the surface ElectroMyoGraphy (sEMG) is widely used as a biomimetic FES control method [12]–[15], leveraging time-domain parameters extracted from the sEMG signal. However, this operation requires signal digitization and embedded feature processing, impacting on power consumption and transmission performance. In order to lighten these tasks, we proposed the Average Threshold Crossing (ATC) parameter, computed by processing the raw sEMG signal directly in hardware, as a part of the analog front-end, over fixed-length (i.e., 130 ms) observation windows [16]. Due to the high correlation between ATC and the exerted muscle force [17], it results suitable for driving the FES [18], [19]. Besides the custom-designed embedded acquisition devices [16] and the electrical stimulator [26], our ATC-FES system includes a control platform, implemented on a computer [20], [21], for computing the FES profiles.

Since the early experiments conducted on single-channels tasks [19]–[21], our main goal has been to extend the applicability of the ATC paradigm to the control of multi-channel FES. To this end, one of the main issue that we faced was the calibration of the ATC-FES system. Generally, in FES systems the proper customization of the electrical stimulation is a crucial step, because it can reduce the fatigue and optimize the force output [22]. A common methodology to calibrate FES consists in tuning the stimulation intensity according to the individual response of each involved muscle [6]–[8], [14], [23], modulating either the pulse width or the amplitude and maintaining fixed the pulse frequency: the current intensity is increased until it elicits muscle contraction without causing pain in the patient. This process can be easily conducted in single-channel application, but it may be under-performing in multi-channels cases, since it does not consider the inter-muscles synergies. In our system, the ATC-FES relationship, implemented on the control platform, is linearly mapped by a Look-Up Table (LUT) [20], [21], which is returned as a result of two independent calibration sub-routines: 1) the maximum ATC is computed as the median value among the peaks produced by voluntary movement repetitions; 2) the maximum current intensity is found stimulating the patient with a repetitive pyramidal-shaped pattern (PYR), progressively increasing its maximum. The PYR ramps from zero to the peak amplitude with 2 mA steps and decline symmetrically, providing a gradual stimulation delivery. Despite the overall simplicity of this calibration approach, which can be easily implemented in single-channel tasks, it may not scale well in a multi-channel scenario. In fact, the overall difficulty in reproducing multi-joint functional movements with a non-specific stimulation pattern implies the FES calibration to be executed channel-by-channel. Therefore, we investigated the possibility of using a biomimetic stimulation to enable the multichannel calibration and improve the FES parameters selection, since, at the best of our knowledge, no previous works explored this perspective.

In this context, we propose the novel Profile Extraction (PE) algorithm, which redefines the maximum ATC calibration protocol to extract a biomimetic profile highly correlated with the driving muscles activity. The algorithm is general enough so that the extracted pattern could be broadly used to deliver a remote biomimetic stimulation to the patient avoiding the simultaneous intervention of a controller subject. However,

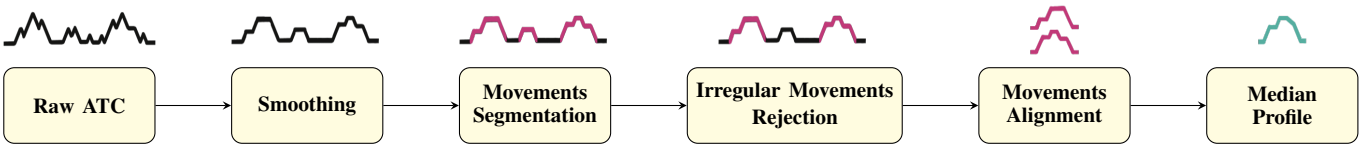

Fig. 1. The PE algorithm is organized in a pipeline, which starts from ATC raw data and returns a median ATC profile, highly correlated with the original sequence. For the sake of clarity, the figure shows the PE performed on a single-channel ATC sequence, but the pipeline is actually designed to work on multiple channels simultaneously.

specifically, in this work we focused on the implementation of the PE algorithm in the calibration routines. An experimental campaign was conducted in this regard, comparing the novel calibration with the former one based on the PYR profile, and evaluating for both methods the impact of selected parameters on therapist-patient movements repeatability during the FES sessions performed in single-channel and multi-channel scenarios.

II. Profile Extraction Algorithm

The PE algorithm is structured as a processing pipeline implemented into the ATC maximum calibration phase (Fig. 1): while the therapist performs repetitions of a functional task, raw ATC values received from the acquisition channels undergo a smoothing stage (Section II-A), reducing the influence of background noise. Then, the smoothed data sequences associated with actual muscle contractions are segmented in real-time (Section II-B), producing a set of two-dimensional arrays (*movement* matrices), in which any row corresponds to an acquisition channel. Once the user stops the acquisition, a selection step (Section II-C) is performed to preserve only those *movements* that show higher mutual similarity. In the fourth step, the remaining data segments are processed to extract the final profile (Section II-D). The PE algorithm has been developed using the Python programming language to be easily integrated into the existing control platform software of the ATC-FES system [21].

A. Smoothing

Despite the intrinsic robustness of the ATC technique to several alterations [24], the raw ATC data have to be regularized to smooth ATC sequences and reduce the number of spurious TC events, which could affect the signal baseline depending on the environmental conditions. In each channel, incoming ATC data undergo median filtering, where the number of data involved in the smoothing operation is defined by the window width parameter (in this work set to 3 after preliminar analyses).

B. Movements Segmentation

The *movements* segmentation process detects ongoing muscle contractions by checking iteratively if channels exhibit either an individual or a group activity (Fig. 2):

- A channel (ch) exhibits an individual activity when the sequence of the last N ATC data contains all non-zero elements and at least a peak value higher than 2 events. The parameter N represents the minimum length of an active sequence in terms of ATC samples and must be set according to the typical *movement* duration. We set N equal to 3, sensing voluntary muscle activations that last at least 390 ms.
- The group activity is defined when the number of channels synergistically activated over the total number overcomes a predefined parameter called Group Factor Threshold (*GFT*). The *GFT* value ranges from 0 to 1 and quantifies the inter-channel dependence.

The latter condition defines the onset of a functional *movement*. The adoption of a non-zero *GFT* parameter helps to prevent failures due to the presence of unstable channels. On the other hand, the individual activity is sufficient to define the *movement* onset (*GFT* = 0) when investigated channels do not exhibit a synergistic relationship. During the *movement* execution, incoming ATC values from all channels are appended to *movement* matrix rows. The end of the *movement* sequence is defined when the group activity condition is no more satisfied for 10 consecutive iterations. The number of columns of the resulting matrix corresponds to the length of the *movement* (L).

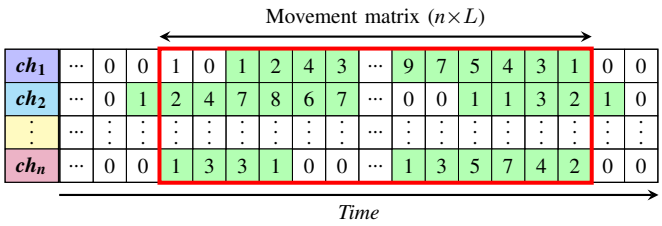

Fig. 2. Example of *movement* segmentation performed on n acquisition channels. Row sequences marked in green represent channels activations, while the red box segments the multi-channel sequence which satisfies the *GFT* condition ($GFT = 2/n$).

C. Irregular Movements Rejection

The Irregular Movement Rejection (*IMR*) step compares all the possible combinations of *movement* segments and rejects those that exhibit the lower mutual similarity. This process assumes that the execution of repetitive tasks produces reproducible activation patterns [25].

The overall similarity between two different *movement* matrices, X and Y, is expressed by the Similarity Index (SI_{XY}).

This scalar parameter, ranging from 0 to 1, is computed as the maximum of the product between the Channels Correlation matrix CC_{XY} and the weight vector W_{XY}, as reported in (1):

$$SI_{XY} = \max_{\tau} \; CC_{XY}^{T} \; W_{XY} \tag{1}$$

$$CC_{XY}[ch, \tau] = \frac{\sum_m X_{ch}[m+\tau] Y_{ch}[m]}{\max(|X_{ch}|_2^2, |Y_{ch}|_2^2)} \tag{2}$$

$$W_{XY}[ch] = \frac{\sum_k X[ch,k] + \sum_m Y[ch,m]}{\sum_{ch}(\sum_k X[ch,k] + \sum_m Y[ch,m]))} \tag{3}$$

The rows of the CC_{XY} matrix, defined in (2), contain the Normalized Channel-wise Cross-correlation (NCC) between X and Y, which provides the measure of channel-by-channel similarity as a function of the relative lag (τ). We defined the NCC with an unusual normalization factor to strengthen its sensitivity to differences in pattern and intensity, returning the maximum value (NCC = 1) only if the two *movements* are identical. The W_{XY} vector, defined in (3), quantifies the contribution of each channel to the whole *movement* with values from 0 to 1.

Similarity matrix						
vs	1	2	3	4	5	6
1	1.00	0.92	0.58	0.85	0.91	0.50
2	0.92	1.00	0.57	0.91	0.94	0.48
3	0.58	0.57	1.00	0.62	0.54	0.84
4	0.85	0.91	0.62	1.00	0.90	0.52
5	0.91	0.94	0.54	0.90	1.00	0.46
6	0.50	0.48	0.84	0.52	0.46	1.00

$\downarrow SI < 0.7$

# Low Similarity Indices						
#	2	2	4	2	2	4

$\downarrow \geq 2.5$

Irregular movements: 3-6

Fig. 3. Example of *IMR* process: six *movements* are compared, producing a 6×6 SM. SI values lower than SI_{min} = 0.7 are marked in red, representing the low similarities. A *movement* compared with the other five is classified as irregular if it exhibits a number of low similarities higher than $\frac{N^\circ \; Movements-1}{2}$ = 2.5. In the Example, the algorithm has rejected two irregular *movements* indexed by numbers 3 and 6.

The Similarity Matrix (SM) is then built by computing SI for all the *movement* combinations. In this symmetrical matrix (Fig. 3), rows and columns are associated with different *movements*, and each pair of coordinates points to the SI of a specific *movements* combination. The τ values that maximize each SI are stored into an analogous anti-symmetrical matrix, called Displacement Matrix (DM). The SM is then used for detecting irregular *movements*: each SI is compared with a fixed threshold value SI_{min} in order to determine if the *movements* to which it refers are similar ($SI \geq SI_{min}$) or different ($SI < SI_{min}$). The process selectivity can be adjusted by tuning SI_{min}. After preliminary experiments, we set it equal to 0.7, providing good similarity discrimination in single-channel and multi-channel applications.

A *movement* is considered irregular when exhibits a low similarity with at least the half of the others ($\frac{N^\circ \; Movements-1}{2}$). This operation is repeated until only regular *movements* remain in the collection, correcting iteratively both the SM and DM.

D. Movements Alignment and Profile Extraction

All the *movements* are aligned before extracting the final profile, stacking their matrices into a three-dimensional array. The *movement* with the highest CI values is selected as the reference. Other matrices are shifted along rows, using τ values contained into the column of DM indexed by the reference *movement*, and equalizing their dimensions through zero-padding. The resulting array is used to extract the final multi-channel profile, performing the median operation across the aligned matrices (Fig. 4).

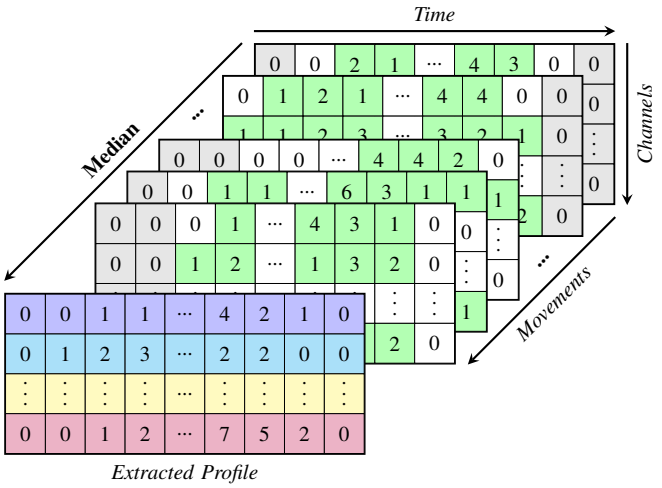

Fig. 4. Example of *movements* alignment: *movement* matrices are aligned, maximizing the mutual cross-correlation. Columns marked in gray are added to equalize matrices dimension. Sequences highlighted in green represents channels' activity.

III. Experimental Tests

The impact of the biomimetic PE profile on the selection of the FES current intensity was evaluated through the comparison with the previously adopted calibration methodology, i.e., PYR profile. The protocol, approved by the Bioethics Committee of Università degli Studi di Torino with the experimental code 445154, was based on a previous work [21]. Two target exercises, with a different number of channels, were studied:

- The Elbow Flexion (EF) was selected as single-channel (SCH) movement for validating the use of PE in a simple tasks, where the PYR approach was previously adopted [19]–[21]. It starts with the subjects seated with the forearm in a supine position and the elbow leaning on a table; the stimulation of the *biceps brachii* induces

the flexion of the elbow joint, maintaining the humeral segment in position.

- A dual-channel (DCH) task was selected for testing the effectiveness of PE on an simple multi-channel application. It starts with the therapist seated in front of a table on which there is a bottle (720 g), placed in line with the sternum and at the 95% of the maximum reachable distance of the therapist's arm; then, s/he brings the bottle to the mouth, mimicking the drinking action; the exercise ends with the therapist returning to the initial rest position after the bottle release. For the sake of simplicity, this functional task can be considered the composition of two simpler movements: the Humerothoracic Elevation (HE) and the Elbow Flexion (EF), controlled by the *anterior deltoid* and *biceps brachii,* respectively. In contrast to the SCH task, the EF angle is susceptible to the dynamics of both the forearm and humerus segment. Therefore, the selection of the proper stimulation current is particularly crucial for achieving the right movement execution.

Following the same approach reported in [21], the protocol was organized in experimental trials conducted on 8 healthy subjects (4 males and 4 females, aged between 24 and 27), which provided their informed consent. In each trial, a therapist-patient couple undergoes the calibration routines followed by 3 online training sessions, during which the therapist repeats the target exercise 10 times with 10 s of inter-repetition pause, driving the electrical stimulation to the patient in real-time. Each couple performed an experimental trial for each calibration method and functional exercise, for a total of 4 trials. The trials related to the same calibration strategy and different exercises were separated by 15 min of inter-trials pause. Instead, the trials related to different calibrations were performed in different days. We employed the HASOMED® RehaTrode [26] (5 cm×9 cm) as stimulation electrodes, placed in standardised positions reported in [27], [28], taking care to perform a proper skin preparation and apply a conductive gel on electrode surface. During the training sessions, body movement trajectories of the therapist and patient were captured using the Vicon motion tracking system configured with 12 cameras. Then, we computed two parameters for their comparison: the maximum value of the normalized cross-correlation (ρ_{max}) and the onset Delay (D) for each movement execution [21]. Additionally, the normalized Root Mean Square Error (*nRMSE*) was computed to quantify the difference between therapist-patient trajectories. In the DCH exercise, a single D per movement was extracted, joining the information of the two joints. For each subject, the outcomes of movement replicates were summarized in average results.

Experimental results (ρ_{max} and *nRMSE*) for the PE and PYR calibration are shown in Fig. 5:

- Considering the SCH task, the PE case produced a 2 % increase in median ρ_{max} (Fig. 5-(a): $\rho_{max\text{PE}} = 0.98$; $\rho_{max\text{PYR}} = 0.96$), a decrease in median *nRMSE* (Fig. 5-(d): $nRMSE_{\text{PE}} = 0.23$; $nRMSE_{\text{PYR}} = 0.26$), and a decrease in median D ($D_{\text{PE}} = 0.5$ s; $D_{\text{PYR}} = 0.65$ s).

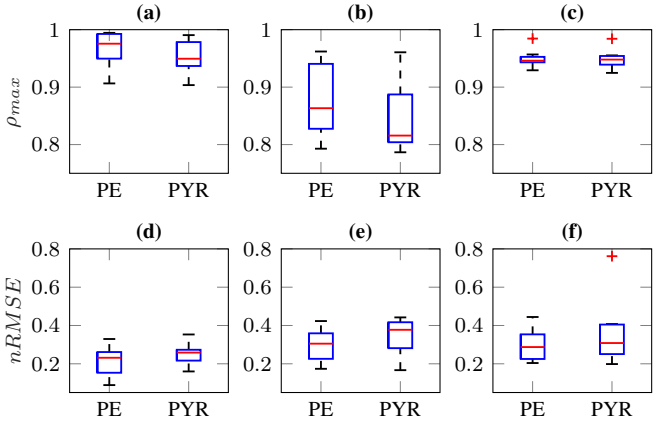

Fig. 5. Box plots representing the average ρ_{max} and *nRMSE* between therapist and patient trajectories divided among joint and exercise types: (a) EF-ρ_{max}-SCH; (b) EF-ρ_{max}-DCH; (c) HE-ρ_{max}-DCH; (d) EF-*nRMSE*-SCH; (e) EF- *nRMSE*-DCH; (f) HE-*nRMSE*-DCH.

- Regarding the DCH composite task, the PE calibration produced a 3.6 % increase in median ρ_{max} (Fig. 5-(b): $\rho_{max\text{PE}} = 0.86$; $\rho_{max\text{PYR}} = 0.83$), and a decrease in median *nRMSE* (Fig. 5-(e): $nRMSE_{\text{PE}} = 0.30$; $nRMSE_{\text{PYR}} = 0.38$) for the EF trajectory. Similar median performances came up from the comparison of the HE trajectory (Fig. 5-(c): $\rho_{max\text{PE,PYR}} \simeq 0.95$; (f): $nRMSE_{\text{PE,PYR}} \simeq 0.30$) and median D values ($D_{\text{PE,PYR}} \simeq 0.49$ s).

The two-sided Wilcoxon signed rank test was performed to investigate significant effects of the calibration type on the average comparison results. Considering the preliminary nature of these experiments and the limited number of participants, while we did not expect any statistically significant difference in simpler movements, a statistically significant difference between calibrations ($p < 0.05$) emerged from the more complex multi-channel composite DCH task, where the use of PE strategy reduced the *nRMSE* between EF trajectories of therapist and patient ($p = 0.039$).

IV. Conclusion

This work proposes an algorithm for extracting an event-driven activation profile highly correlated with the driving muscle activity, with the aim of enabling a fully-remote delivery of the biomimetic stimulation and scaling the calibration routines to multi-channel applications. The novel calibration technique was tested through an experimental protocol, comparing the resulting stimulation performance, in terms of movement repeatability, with the former calibration. The results have shown that the introduction of the PE methodology produced an increase of similarity between therapist-patient trajectories, especially for the elbow joint. These tests represented the preliminary attempts to calibrate and stimulate a coordinated multi-channel movement using our event-driven ATC-FES system. Starting from these promising results, the PE algorithm opens new perspectives to scale up the system to control more complex functional tasks, increasing the number of operating channels.

REFERENCES

[1] K. Masani and M. R. Popovic, "Functional electrical stimulation in rehabilitation and neurorehabilitation," in *Springer handbook of medical technology*. Springer, 2011, pp. 877–896.

[2] D. Ming, D. Yuan, Y. Li, M. Xu, X. An, W. Wang, H. Qi, B. Wan, W. Wang, and R. Abboud, "Neuroprosthesis system for lower limbs action based on functional electrical stimulation," in *2011 International Conference on Electrical and Control Engineering*, 2011, pp. 4583–4586.

[3] C. E. King, P. T. Wang, C. M. McCrimmon, C. C. Chou, A. H. Do, and Z. Nenadic, "The feasibility of a brain-computer interface functional electrical stimulation system for the restoration of overground walking after paraplegia," *Journal of neuroengineering and rehabilitation*, vol. 12, no. 1, pp. 1–11, 2015.

[4] N. M. Kapadia, V. Zivanovic, J. Furlan, B. C. Craven, C. McGillivray, and M. R. Popovic, "Functional electrical stimulation therapy for grasping in traumatic incomplete spinal cord injury: randomized control trial," *Artificial organs*, vol. 35, no. 3, pp. 212–216, 2011.

[5] S. C. McGie, J. Zariffa, M. R. Popovic, and M. K. Nagai, "Short-term neuroplastic effects of brain-controlled and muscle-controlled electrical stimulation," *Neuromodulation: Technology at the Neural Interface*, vol. 18, no. 3, pp. 233–240, 2015.

[6] A. Cuesta-Gómez, F. Molina-Rueda, M. Carratala-Tejada, E. Imatz-Ojanguren, D. Torricelli, and J. C. Miangolarra-Page, "The use of functional electrical stimulation on the upper limb and interscapular muscles of patients with stroke for the improvement of reaching movements: A feasibility study," *Frontiers in neurology*, vol. 8, p. 186, 2017.

[7] P. Müller, A. J. Del Ama, J. C. Moreno, and T. Schauer, "Adaptive multichannel FES neuroprosthesis with learning control and automatic gait assessment," *Journal of neuroengineering and rehabilitation*, vol. 17, no. 1, pp. 1–20, 2020.

[8] S. Ferrante, N. Chia Bejarano, E. Ambrosini, A. Nardone, A. M. Turcato, M. Monticone, G. Ferrigno, and A. Pedrocchi, "A personalized multi-channel FES controller based on muscle synergies to support gait rehabilitation after stroke," *Frontiers in neuroscience*, vol. 10, p. 425, 2016.

[9] A. H. Do, P. T. Wang, C. E. King, A. Abiri, and Z. Nenadic, "Brain-computer interface controlled functional electrical stimulation system for ankle movement," *Journal of neuroengineering and rehabilitation*, vol. 8, no. 1, pp. 1–14, 2011.

[10] N. Lan, C. M. Niu, M. Hao, C.-H. Chou, and C. Dai, "Achieving neural compatibility with human sensorimotor control in prosthetic and therapeutic devices," *IEEE Transactions on Medical Robotics and Bionics*, vol. 1, no. 3, pp. 122–134, 2019.

[11] X. Zhao, Z. Wang, R. Xu, and D. Ming, "A real-time sEMG-based control strategy and system for contralaterally controlled functional electrical stimulation," in *2021 IEEE International Conference on Robotics and Biomimetics (ROBIO)*, 2021, pp. 785–789.

[12] Z. Lou, P. Yao, and D. Zhang, "Wireless master-slave FES rehabilitation system using sEMG control," in *International Conference on Intelligent Robotics and Applications*. Springer, 2012, pp. 1–10.

[13] Y. Zhou, Y. Fang, K. Gui, K. Li, D. Zhang, and H. Liu, "sEMG bias-driven functional electrical stimulation system for upper-limb stroke rehabilitation," *IEEE Sensors Journal*, vol. 18, no. 16, pp. 6812–6821, 2018.

[14] C. M. Niu, Y. Bao, C. Zhuang, S. Li, T. Wang, L. Cui, Q. Xie, and N. Lan, "Synergy-based FES for post-stroke rehabilitation of upper-limb motor functions," *IEEE Transactions on Neural Systems and Rehabilitation Engineering*, vol. 27, no. 2, pp. 256–264, 2019.

[15] B. A. Osuagwu, E. Whicher, and R. Shirley, "Active proportional electromyogram controlled functional electrical stimulation system," *Scientific reports*, vol. 10, no. 1, pp. 1–15, 2020.

[16] F. Rossi, A. Mongardi, P. Motto Ros, M. Ruo Roch, M. Martina, and D. Demarchi, "Tutorial: A versatile bio-inspired system for processing and transmission of muscular information," *IEEE Sensors Journal*, vol. 21, no. 20, pp. 22 285–22 303, 2021.

[17] S. Sapienza, M. Crepaldi, P. Motto Ros, A. Bonanno, and D. Demarchi, "On integration and validation of a very low complexity ATC UWB system for muscle force transmission," *IEEE Transactions on Biomedical Circuits and Systems*, vol. 10, no. 2, pp. 497–506, 2016.

[18] F. Rossi, P. Motto Ros, S. Sapienza, P. Bonato, E. Bizzi, and D. Demarchi, "Wireless low energy system architecture for event-driven surface electromyography," in *International Conference on Applications in Electronics Pervading Industry, Environment and Society*. Springer, 2018, pp. 179–185.

[19] F. Rossi, P. Motto Ros, S. Cecchini, A. Crema, S. Micera, and D. Demarchi, "An event-driven closed-loop system for real-time FES control," in *2019 26th IEEE International Conference on Electronics, Circuits and Systems (ICECS)*. IEEE, 2019, pp. 867–870.

[20] F. Rossi, P. Motto Ros, R. M. Rosales, and D. Demarchi, "Embedded bio-mimetic system for functional electrical stimulation controlled by event-driven sEMG," *Sensors*, vol. 20, no. 5, p. 1535, 2020.

[21] A. Prestia, F. Rossi, A. Mongardi, P. Motto Ros, M. Ruo Roch, M. Martina, and D. Demarchi, "Motion analysis for experimental evaluation of an event-driven FES system," *IEEE Transactions on Biomedical Circuits and Systems*, vol. 16, no. 1, pp. 3–14, 2022.

[22] B. M. Doucet, A. Lam, and L. Griffin, "Neuromuscular electrical stimulation for skeletal muscle function," *The Yale journal of biology and medicine*, vol. 85, no. 2, p. 201, 2012.

[23] E. M. Camilo, J. A. M. Gutiérrez, O. P. Ramírez, J. G. Martínez, A. V. Hernández, and L. L. Salas, "A functional electrical stimulation controller for contralateral hand movements based on EMG signals," in *2020 17th International Conference on Electrical Engineering, Computing Science and Automatic Control (CCE)*, 2020, pp. 1–6.

[24] P. Motto Ros, M. Paleari, N. Celadon, A. Sanginario, A. Bonanno, M. Crepaldi, P. Ariano, and D. Demarchi, "A wireless address-event representation system for ATC-based multi-channel force wireless transmission," in *5th IEEE International Workshop on Advances in Sensors and Interfaces IWASI*. IEEE, 2013, pp. 51–56.

[25] B. Larsson, C. Karlberg, J. Elert, and B. Gerdle, "Reproducibility of surface EMG during dynamic shoulder forward flexions: a study of clinically healthy subjects," *Clinical Physiology*, vol. 19, no. 5, pp. 433–439, 1999.

[26] HASOMED GmbH, *Operation Manual RehaStim2, RehaMove2 - User Guide*, September 2012.

[27] FES electrode placements: Upper body. Accessed: August 30, 2022. [Online]. Available: https://www.ualberta.ca/steadward-centre/media-library/altastim/fes_electrode_placement_upper_body-2018.pdf

[28] HASOMED GmbH, *RehaMove, Functional electrical stimulation - FES applications*, June 2015.